Defect-Rich Carbon Supported Pt Nanoparticles via Joule Heating for Enhanced Oxygen Reduction

Muhammad Hamza,[a] Song Lu,[b] Xueyan Jiao,[a] Bobo Zhao,[a] Wei Wang,[a] Bingchen Yin,[a] Lipiao Bao,[a] Xing Lu[a] and Kun Guo*[a]

[a] *State Key Laboratory of New Textile Materials and Advanced Processing, and School of Materials Science and Engineering, Huazhong University of Science and Technology, Wuhan 430074, China*

[b] *Institute of New Energy, School of Chemistry and Chemical Engineering, Shaoxing University, Shaoxing 312000, China*

*Corresponding author:

K. Guo (guok@hust.edu.cn)

Table of Contents

Experimental Section

1. Chemicals

All chemicals were purchased unless otherwise indicated and used as received without further treatment. Platinum (II) acetylacetonate ($Pt(acac)_2$, ≥98%), potassium hydroxide (KOH, ≥85.0%), sulfuric acid (H_2SO_4, 96%), perchloric acid ($HClO_4$, 70%), toluene (≥99.5%), ethanol (99.7%), and acetone (≥99%) were ordered from Sinopharm Chemical Reagent Co., Ltd. Nafion ionomer solution (5 wt.%) and platinum on activated carbon (20 wt.% Pt/C) were obtained from Sigma Aldrich. C_{60} fullerene (99%) was purchased from Xiamen Funano New Material Technology Co., Ltd. Ketjenblack EC-600 JD (KB) carbon black was ordered from AkzoNobel. Carbon nanotubes (CNT, multi-walled, 95%, length of 10–30 μm and diameter of 10–20 nm) were received from Nanjing XFNANO Materials Tech Co., Ltd. Graphitic nanoplatelets (GNPs, product No. HXGOP-90) were supplied by Wuhan Hanene Technology Co., Ltd. Deionized water (18.2 MΩ·cm) was used in all the experiments.

2. Materials Synthesis

Synthesis of fullerene-derived carbon (FC)

For the preparation of FC, 200 mg of C_{60} and 2.4 g of KOH were dissolved in 100 mL of toluene and 50 mL of ethanol, respectively. The KOH solution was then poured into the C_{60} solution and stirred vigorously for 2 h. Afterwards, the mixture was stirred and heated at 115 °C until the organic solvents were completely evaporated. The collected dark brown powder was then transferred to a ceramic cauldron and calcined at 700 °C for 30 minutes in a nitrogen stream in a tube furnace. The resulting black powder was manually ground and dispersed in 0.5 M H_2SO_4 for 8 h to remove residual alkali and impurities. The product was collected in a centrifuge and washed with ultra-pure water until the solution became pH-neutral. The dry sample was then heated for a second time in a nitrogen stream at 900 °C for 1 h to obtain the final powder product of FC.

Synthesis of carbon supported Pt nanoparticles (NPs)

For the preparation of FC supported Pt NPs (Pt/FC), 10 mg of $Pt(acac)_2$ was fully dissolved in 10 mL of acetone, into which 43.8 mg of FC (a nominal Pt loading of 10 wt.%) was dispersed to form a uniform dark black suspension. The nominal loading of Pt on FC was 10 wt.%. Then, acetone was removed using a rotary evaporator and the dry black powder was thoroughly grounded. The fine powder was rapidly heated to 1830 ± 70 °C in 1.5s using a Joule heating furnace (Hefei In-situ Technology Co., LTD.) at a

voltage of 40 V and a current of 375 A to obtain Pt/FC. Pt/KB, Pt/CNT, and Pt/GNP were prepared via the same procedures except that FC was replaced by the same amount of KB, CNT, and GNP, respectively.

3. Material Characterization

Transmission electron microscopy (TEM) was carried out on a JEM-2010F (JEOL) electron microscope at an accelerating voltage of 200 kV. A copper grid coated with a thin carbon film was used as the specimen holder. Scanning electron microscopy (SEM) was performed on a Nova NanoSEM 450 (FEI) electron microscope at an accelerating voltage of 10 kV.

X-ray powder diffraction (XRD) was performed to obtain the crystallographic information of the samples. The powder diffraction patterns were recorded on a Malvern Panalytical X-ray diffractometer (Empyrean) using Cu Kα radiation source (λ = 1.5406 Å, 45 kV and 40 mA). Scanning angles for all samples were set in the 2θ range of 5−90° with a step size of 0.01313° and time per step of 120 s. Peaks were indexed to the database established by Joint Committee on Powder Diffraction Standards (JCPDS).

Raman spectrum was acquired using a confocal Raman microscope (LabRAM HR800, Horiba JobinYvon) equipped with an optical microscope, a CCD camera, and an argon ion laser source. The laser provided 0.2 mW power at a wavelength of 532 nm for the exciting line. Integration time was 60 s, number of co-addition was 2, and slit aperture size was 50×1000 μm.

X-ray photoelectron spectroscopy (XPS) analysis was performed on the K-Alpha X-ray photoelectron spectrometer system (Thermo Fisher Scientific) utilizing a monochromatic Al Kα source (1486.69 eV). High-resolution spectra were obtained at a pass energy of 50.0 eV, a step size of 0.1 eV, and a dwell time of 250 ms per step. The analysis spot size was 400 μm. All binding energies were calibrated to the graphitic C 1s peak at 284.8 eV. XPS peaks were deconvolved and curve-fitted on the CasaXPS software using the Gaussian–Lorentzian mix/Lorentzian asymmetric function and Shirley background.

Nitrogen adsorption−desorption measurements were conducted at the liquid nitrogen temperature of 77 K on a Micromeritics TriStar II surface area and porosity analyzer after degassing under vacuum at 80 °C for 12 h using a sample degas system (Micromeritics VacPrep 061). Specific surface area was calculated using the Brunauer–Emmett–Teller (BET) method.

4. Electrochemical Measurements

All the electrochemical measurements were conducted on a CHI760E electrochemical workstation

(Shanghai Chenhua Instruments Co., Ltd., China) and a MSR rotator (Pine Instrument Company, USA) in a standard three-electrode cell at room temperature. A glassy carbon rotating disk electrode (RDE, diameter of 5 mm), an Ag/AgCl in saturated KCl electrode and a platinum foil/graphite rod were used as the working, reference, and counter electrodes, respectively. All the potential given was calibrated to the reversible hydrogen electrode (RHE) according to the Nernst equation $E_{\text{vs RHE}} = E_{\text{vs Ag/AgCl}} + 0.198 + 0.0592 \times \text{pH}$. 0.1 M KOH aqueous solution was used as the electrolyte.

The working electrode was fabricated via the following procedures: 5 mg of the as-prepared catalyst was dispersed in a mixture of 960 μL of ethanol and 40 μL of 5 wt % Nafion solution. The mixture was ultrasonically dispersed for at least 0.5 h to obtain a homogeneous suspension. Then 20 μL of the suspension was taken by a microsyringe and drop-casted onto a clean RDE with an overall loading of 0.25 mg cm^{-2}. The modified RDE was dried naturally in air. Prior to the tests, the electrochemical cell was saturated by purging Ar or O_2 for at least 30 min. The linear sweep voltammetry (LSV) scan potential was set from 1.2 to 0 V, the scan rate was 10 mV s^{-1}, and the rotational speeds were 400–1600 rpm. Before the LSV test, cyclic voltammetry (CV) was conducted for 5 cycles in the potential range of 0–1.2 V at a scan rate of 20 mV s^{-1} to activate the catalyst. CV was also conducted for 3 cycles in the potential range of 0.05–1.0 V at a scan rate of 20 mV s^{-1} in Ar-saturated 0.1 M $HClO_4$ to measure the electrochemically-active surface area (ECSA). Accelerated stress test (AST) was conducted by potential sweeps between 0.6 V and 1.0 V at a scan rate of 100 mV s^{-1}. Long-term durability was measured using the chronoamperometric technique at 0.6 V and 1600 rpm for 20 h.

Kinetic current density (j_K) was calculated according to the following equation:

$$j_K = \frac{j_L \cdot j}{j_L - j} \tag{1}$$

where j and j_L are the measured and diffusion-limited current densities, respectively.

Electron transfer number (n) was calculated according to the Koutecky–Levich (K–L) equation as follows:

$$\frac{1}{j} = \frac{1}{j_L} + \frac{1}{j_K} = \frac{1}{B\omega^{1/2}} + \frac{1}{j_K} \tag{2}$$

$$B = 0.2nFC_0(D_0)^{2/3}\upsilon^{-1/6} \tag{3}$$

where ω is the electrode rotational speed in the unit of rpm, F is the Faraday constant (96,485 C mol^{-1}),

C_0 is the bulk concentration of O_2 in 0.1 M KOH (1.2×10^{-6} mol cm^{-3}), D_0 is the diffusion coefficient of O_2 in 0.1 M KOH (1.9×10^{-5} cm^2 s^{-1}), and υ is the kinetic viscosity of the electrolyte (0.01 cm^2 s^{-1}).

The rotating ring-disk electrode (RRDE) measurements were conducted in O_2-saturated 0.1 M KOH at 1600 rpm and a scan rate of 10 mV s^{-1}. The ring potential was set as 1.3 V. The n value and peroxide yield (HO_2^-) were calculated by the following equations:

$$HO_2^-(\%) = 200 \times \frac{I_r/N}{I_d + I_r/N} \quad (4)$$

$$n = 4 \times \frac{I_d}{I_d + I_r/N} \quad (5)$$

where I_r and I_d are the ring and disk currents, respectively, and N is the current collection efficiency of RRDE (0.37).

ECSA value was determined by integrating of the hydrogen adsorption region integrated from 0.05 V to 0.4 V. The final cycle of a set of three cycles was used for data analysis. The ECSA (m^2 g_{Pt}^{-1}) was calculated using the following equation:

$$ECSA = \frac{Q_H}{q_H \cdot M_{Pt}} \quad (6)$$

where Q_H is the integrated charge for hydrogen adsorption, M_{Pt} is the mass loading of Pt, and q_H equals to 210 μC cm^{-2}, corresponding to the charge of a hydrogen monolayer adsorbed on polycrystalline Pt.

5. Theoretical Calculation Details

The density functional theory (DFT) calculations were conducted with the projector-augmented wave method implemented in the Vienna ab initio Simulation Package.[S1,2] Intact graphene and graphene with a pentagonal defect were employed as the carbon supports, onto which a 12-atom Pt cluster was introduced. A vacuum of 18 Å was imposed in the Z direction. The Perdew-Burke-Ernzerhof within the generalized gradient approximation was utilized as an exchange-correlation functional.[S3] A plane-wave cutoff energy of 450 eV was set for all the computations to describe all atoms' valence electrons. The convergence criterion of energy and force was set to 10^{-4} eV and 0.02 eV $Å^{-1}$, respectively. G-centered 2×2×1 and 4×4×1 k-points grids were chosen for optimization and electronic structure calculations, respectively.

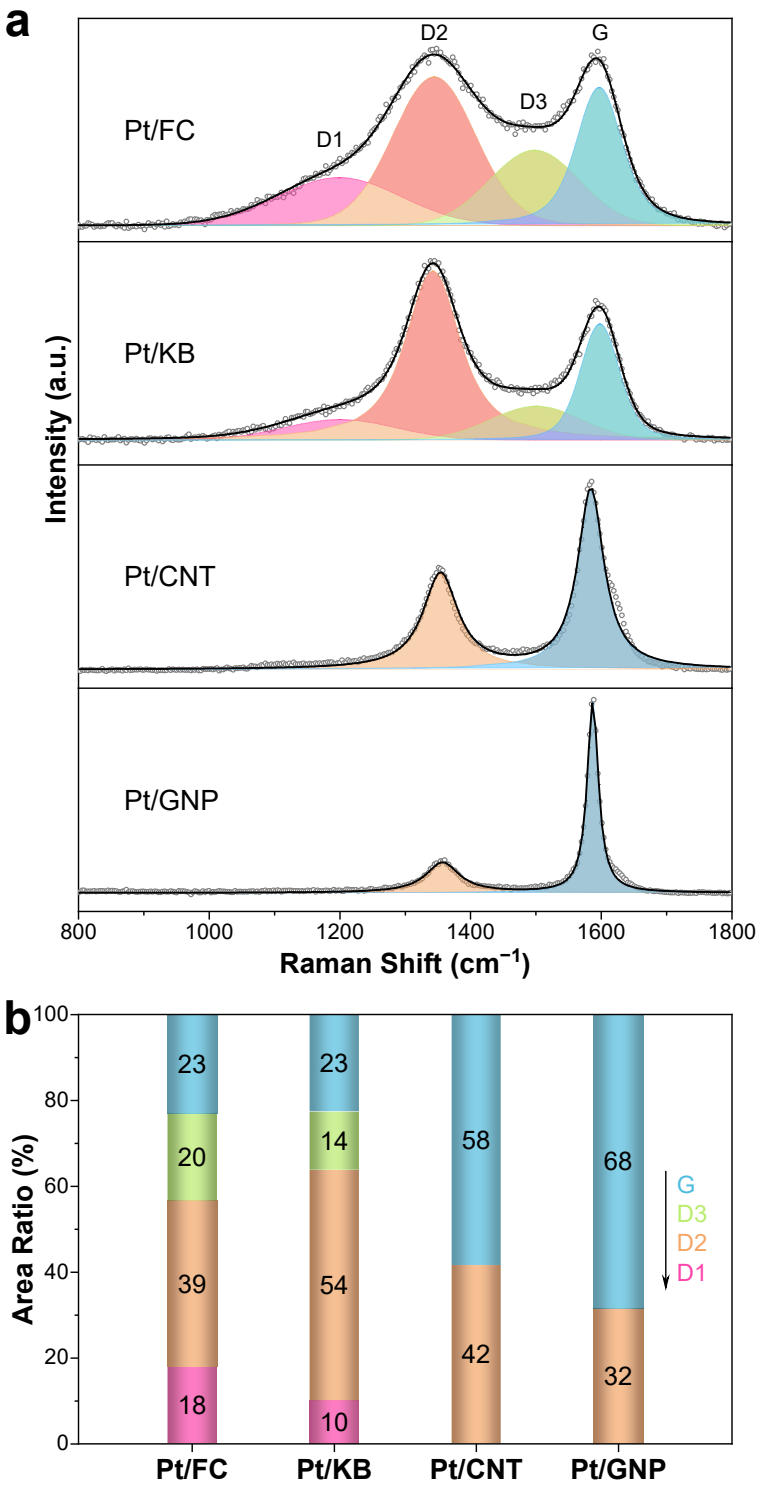

Figure S1. (a) Deconvolution of the Raman spectra of the carbon supported Pt NPs into D1, D2, D3, and G bands. (b) Corresponding areal ratios of the four deconvoluted bands.

The D1 band stems from polyene-like species [S4], the D2 band results from edge-situated C and C(sp^3) atoms [S5,6], and the D3 band originates from pentagons and heteroatoms [S7-9].

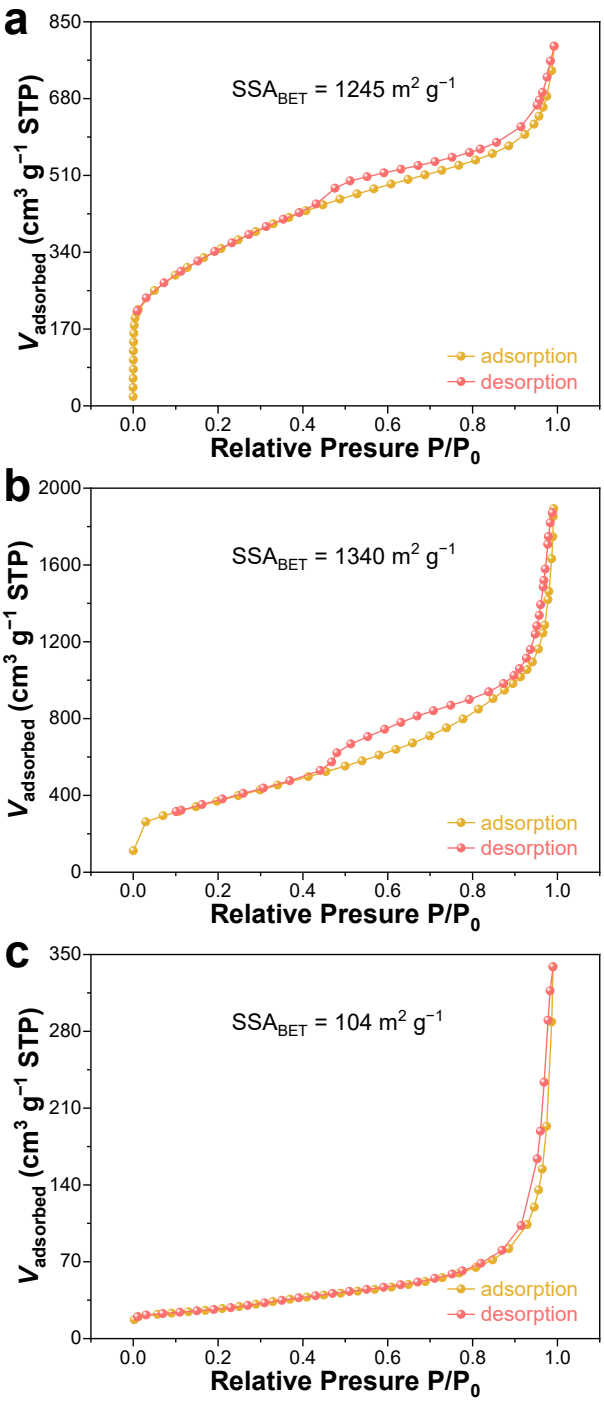

Figure S2. N_2 adsorption–desorption isotherms and corresponding BET SSAs of FC (a), KB (b), and CNT (c).

According to the supplier of GNP, its BET SSA is in the range of 200~300 m^2 g^{-1}.

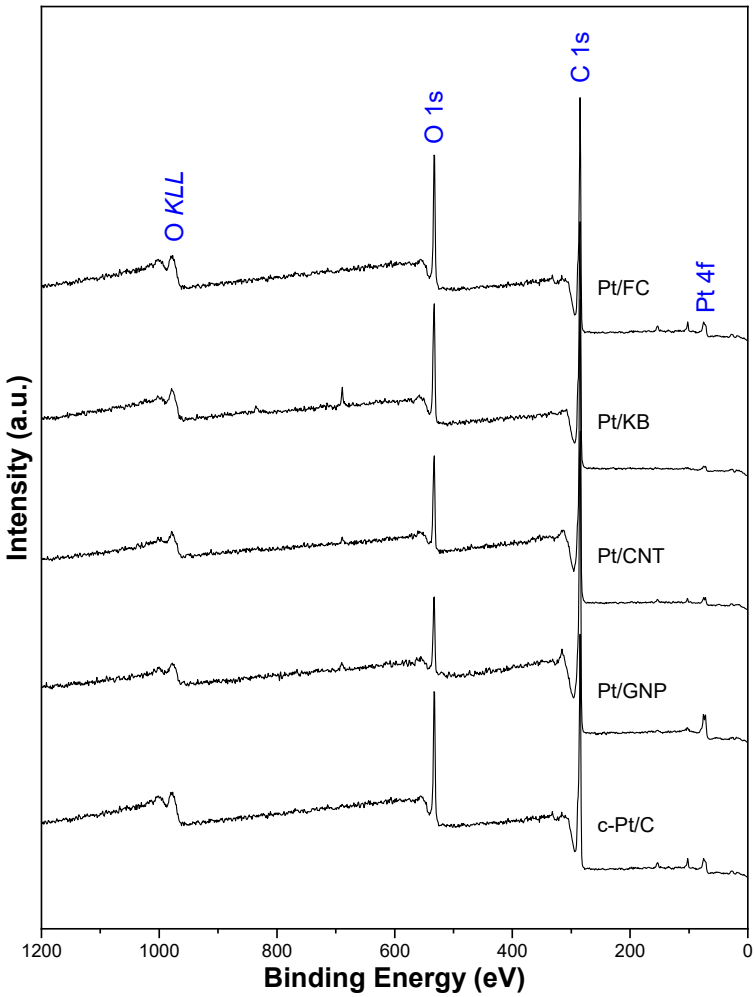

Figure S3. Full-survey XPS spectra of Pt/FC, Pt/KB, Pt/CNT, Pt/GNP, and c-Pt/C.

Table S1. The elemental contents of C and Pt from the XPS measurements.

	C		Pt	
	at.%	wt.%	at.%	wt.%
Pt/FC	99.37	90.66	0.63	9.34
Pt/KB	99.36	90.53	0.64	9.47
Pt/CNT	99.41	91.20	0.59	8.80
Pt/GNP	99.40	91.07	0.60	8.93

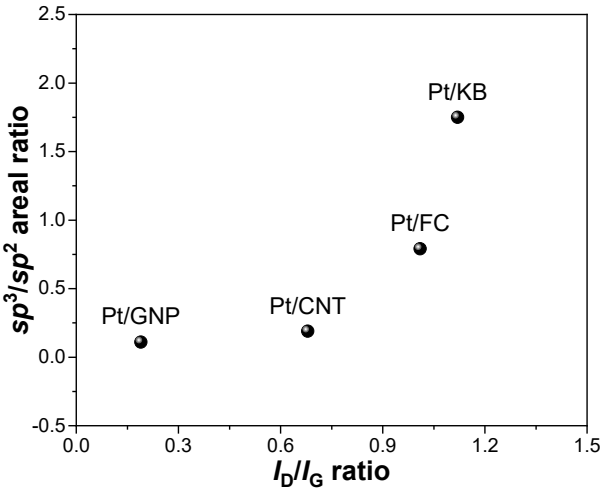

Figure S4. The correlation between I_D/I_G ratio and sp^3/sp^2 areal ratio of Pt/FC, Pt/KB, Pt/CNT, and Pt/GNP.

Table S2. Comparison of ORR activity of Pt/FC in this study with recently reported Pt-based catalysts in alkaline electrolytes.

Catalyst	Electrolyte	$E_{1/2}$ (V vs RHE)	Reference
Pt/FC	0.1 M KOH	0.882	This study
Pt_{NC}/Fe_{SA}-NC	0.1 M KOH	0.86	[S10]
Pt/PCNF	0.1 M KOH	0.927	[S11]
Pt_{SA}–PtCo NCs/N–CNTs-900	0.1 M KOH	0.86	[S12]
Pt@Fe-N-C	0.1 M KOH	0.86	[S13]
Pt_1-CuO_x/Cu	0.1 M KOH	0.92	[S14]
Mn-Pt/NKB	0.1 M KOH	0.89	[S15]
Pt-rich Pt/Ni nanodendrites	1 M KOH	0.88	[S16]
$PtCo_3$/NC	0.1 M KOH	0.82	[S17]
ea-Pt/a-TiO_x/$[Ti_2O]^{2+}\cdot 2e^-$	0.1 M KOH	0.82	[S18]
Pt@Mn-SAs/N-C	0.1 M KOH	0.91	[S19]
Pt/Fe−N−C	0.1 M KOH	0.86	[S20]
Pt_3Co@Pt-SAC	0.1 M KOH	0.86	[S21]
Pt_1-N/BP	0.1 M KOH	0.87	[S22]
SA-PtCoF	1 M KOH	0.88	[S23]

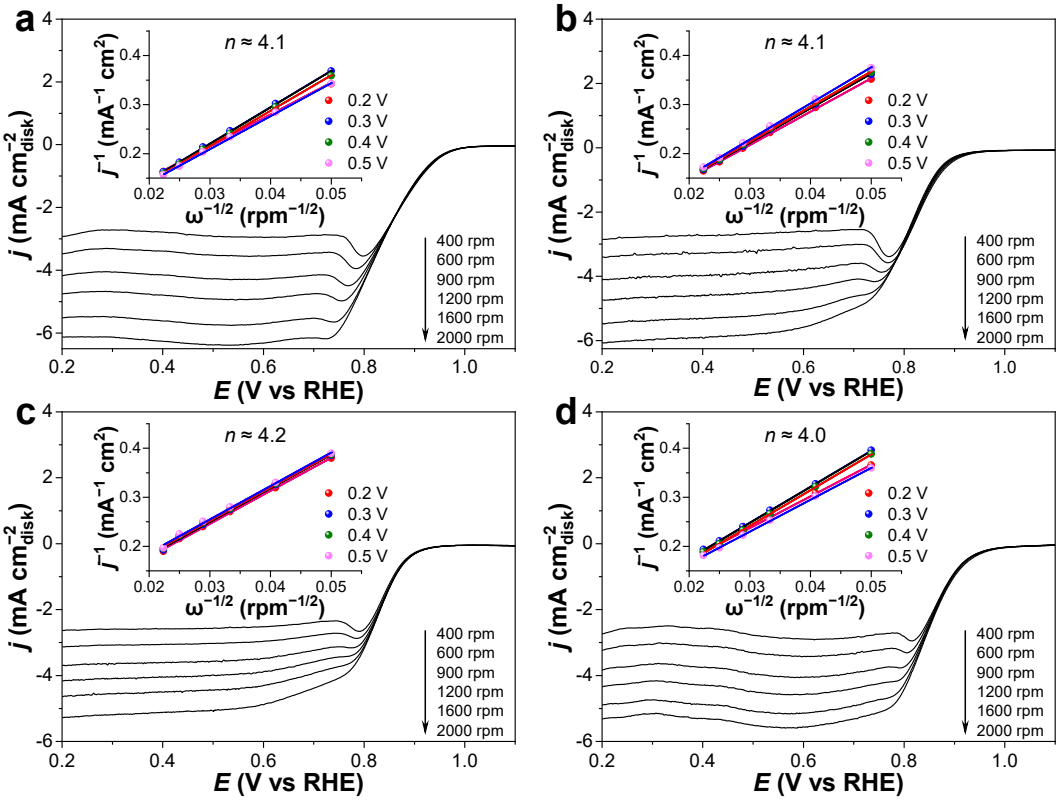

Figure S5. ORR polarization plots at different rotating speeds of 400–2000 rpm and the derived K–L plot (insets) and average *n* values of Pt/KB (a), Pt/CNT (b), Pt/GNP (c), and c-Pt/C (d).

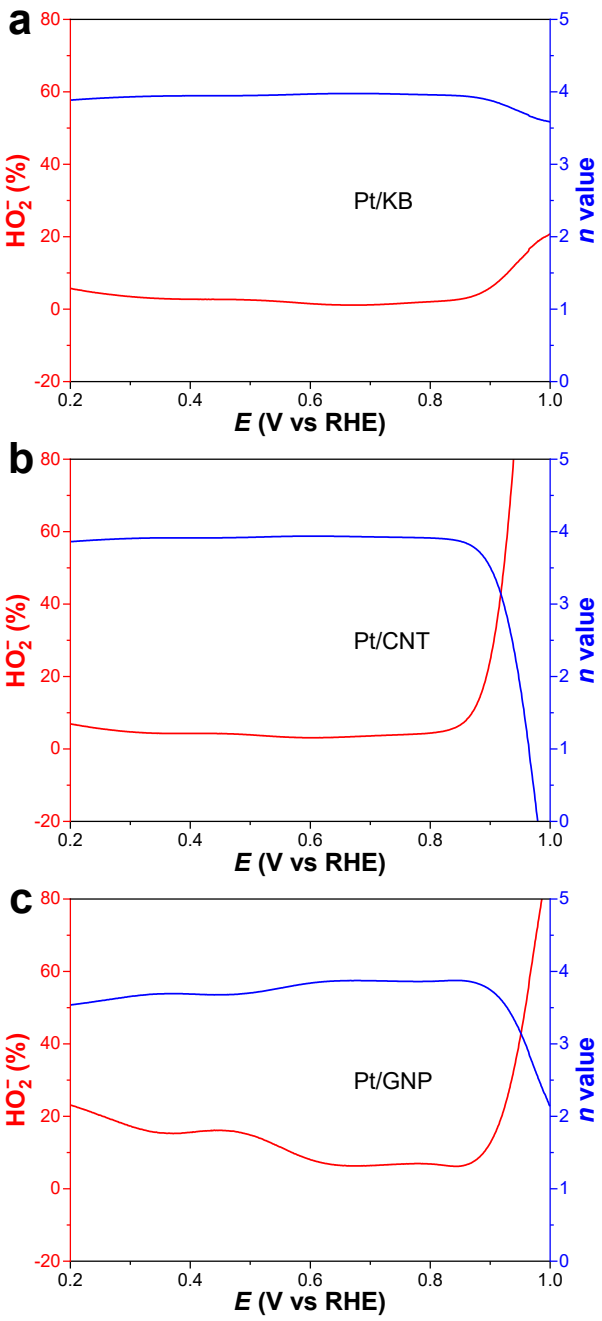

Figure S6. HO_2^- yield and *n* value derived from the RRDE tests of Pt/KB (a), Pt/CNT (b), and Pt/GNP (c).

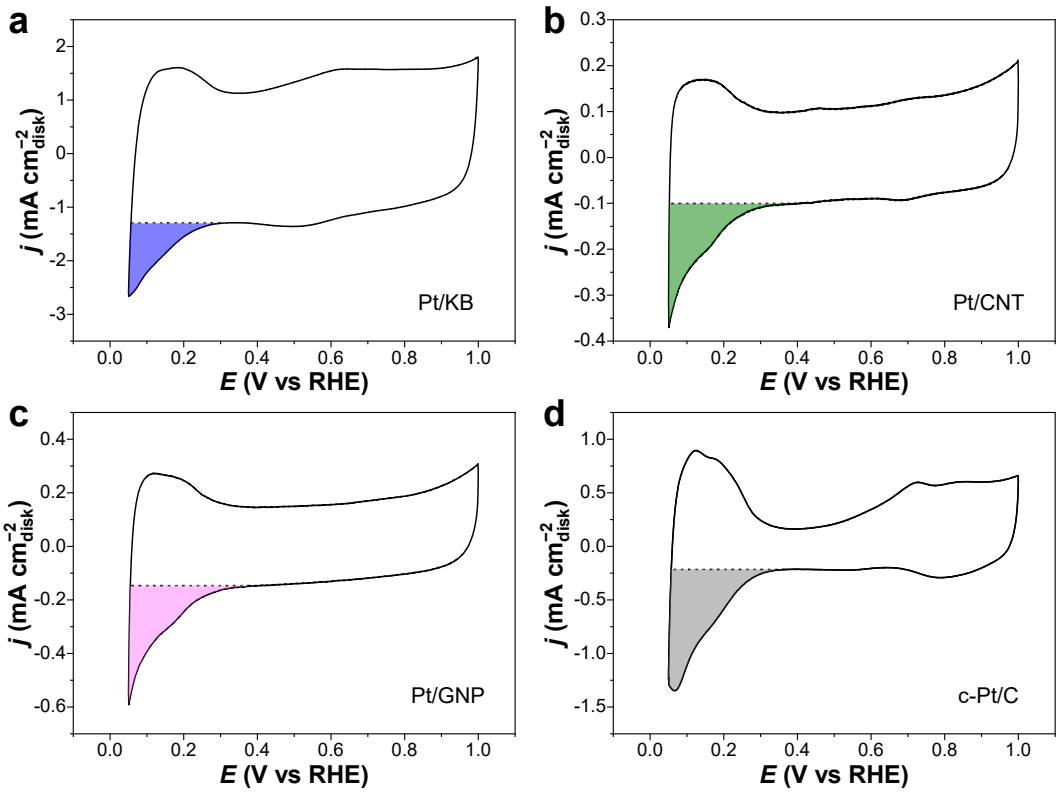

Figure S7. CV curves of Pt/KB (a), Pt/CNT (b), Pt/GNP (c), and c-Pt/C (d) in Ar-saturated $HClO_4$. The colored area denoting the hydrogen adsorption region is integrated for ECSA calculation.

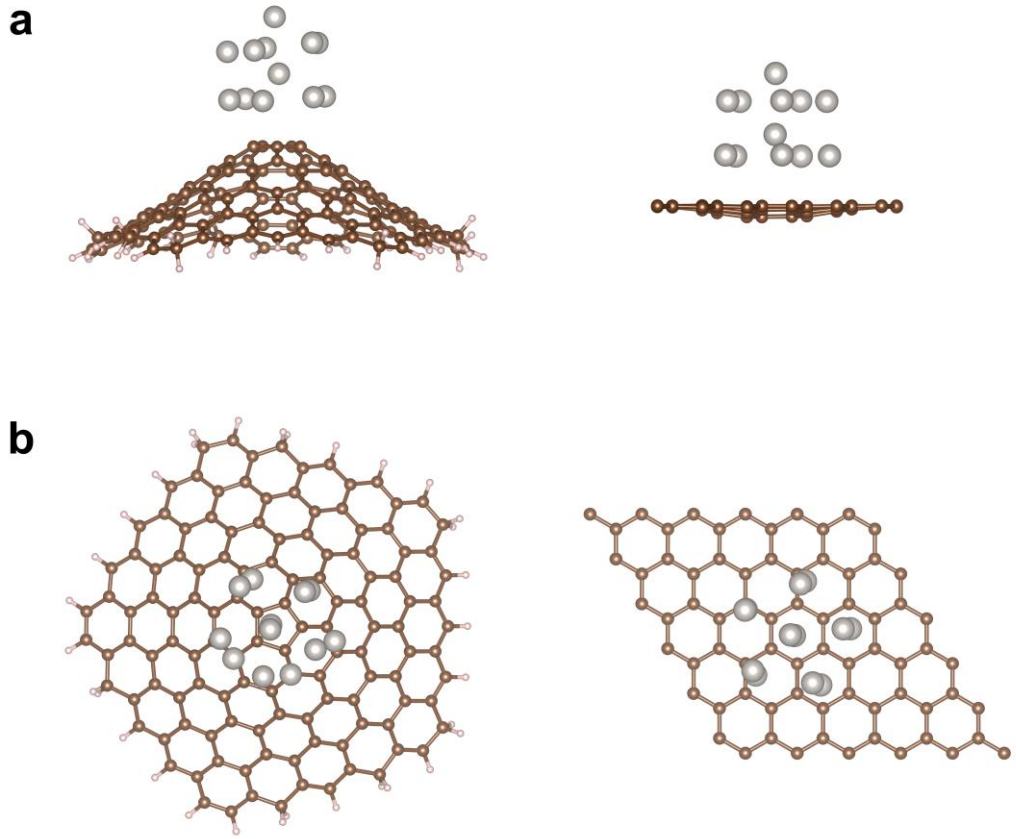

Figure S8. Front (a) and top (b) views of the atomic models of a Pt_{12} cluster supported on graphene with (left) and without (right) a pentagon defect.

Table S3. Comparison of the transferred electron numbers of the five Pt atoms that are adjacent to the graphene support with and without pentagon.

	1st Pt	2nd Pt	3rd Pt	4th Pt	5th Pt
with pentagon	0.07 e^-	0.13 e^-	0.11 e^-	0.11 e^-	0.07 e^-
without pentagon	0.07 e^-	0.10 e^-	0.04 e^-	0.09 e^-	0.05 e^-

References

[S1] G. Kresse, J. Furthmuller, *Phys. Rev. B* **1996**, *54*, 11169.

[S2] G. Kresse, D. Joubert, *Phys. Rev. B* **1999**, *59*, 1758.

[S3] J.P. Perdew, K. Burke, M. Ernzerhof, *Phys. Rev. Lett.* **1996**, *77*, 3865.

[S4] A. Sadezky, H. Muckenhuber, H. Grothe, R. Niessner, U. Pöschl, *Carbon* **2005**, *43*, 1731.

[S5] G. Katagiri, H. Ishida, A. Ishitani, *Carbon* **1988**, *26*, 565.

[S6] Y. Wang, D.C. Alsmeyer, R.L. McCreery, *Chem. Mater.* **1990**, *2*, 557.

[S7] M. Ramm, M. Ata, K.W. Brzezinka, T. Gross, W. Unger, *Thin Solid Films* **1999**, *354*, 106.

[S8] M. Baibarac, L. Mihut, N. Preda, I. Baltog, J.Y. Mevellec, S. Lefrant, *Carbon* **2005**, *43*, 1.

[S9] G. Wu, C.M. Johnston, N.H. Mack, K. Artyushkova, M. Ferrandon, M. Nelson, J.S. Lezama-Pacheco, S.D. Conradson, K.L. More, D.J. Myers, P. Zelenay, *J. Mater. Chem.* **2011**, *21*, 11392.

[S10] C.Y. Du, Z.Q. Ge, L.H. Ouyang, H.Y. Xu, H.Y. Ma, X.T. Wang, Z.Q. Liu, *Angew. Chem. Int. Ed.* **2026**, *65*, e15517.

[S11] Z. Han, W. Deng, Y. Song, H. Cao, Y. Shen, Z. Dang, Z. Zheng, J. Guo, *Carbon* **2026**, *246*, 120950.

[S12] W. Chen, X. Zhu, W. Wei, H. Chen, T. Dong, R. Wang, M. Liu, K. Ken Ostrikov, P. Peng, S.Q. Zang, *Small* **2023**, *19*, 2304294.

[S13] J. Yang, S. Song, Z. Chen, B. Zhang, Y. Guo, Y. Guo, H. Zhang, *J. Mater. Chem. A* **2025**, *13*, 6020.

[S14] W. Zhou, B. Li, X. Liu, J. Jiang, S. Bo, C. Yang, Q. An, Y. Zhang, M.A. Soldatov, H. Wang, S. Wei, Q. Liu, *Nat. Commun.* **2024**, *15*, 6650.

[S15] L. Gao, Y. Song, X. Xu, C. Li, C. Hu, *Nano Res.* **2024**, *17*, 7126.

[S16] S. Ming, S.J. Cobb, M. Rahaman, N. Sammy, E. Reisner, A.E.H. Wheatley, *Adv. Funct. Mater.* **2024**, *34*, 2411006.

[S17] X. Chen, J. Guo, D. Qian, J. Wu, W. Liao, G.I.N. Waterhouse, J. Liu, *Small* **2024**, *20*, 2403894.

[S18] E. Hua, S. Choi, S. Ren, S. Kim, G. Ali, S.J. Kim, W.S. Jang, S. Joo, J. Zhang, S. Ji, Y.S. Cho, J. Kang, T. Song, S. Hong, H. Choi, Y.M. Kim, H. Han, S.W. Kim, *Energy Environ. Sci.* **2023**, *16*, 4464.

[S19] L. Gong, J. Zhu, F. Xia, Y. Zhang, W. Shi, L. Chen, J. Yu, J. Wu, S. Mu, *ACS Catal.* **2023**, *13*, 4012.

[S20] F. Xiao, Y. Wang, G.-L. Xu, F. Yang, S. Zhu, C.-J. Sun, Y. Cui, Z. Xu, Q. Zhao, J. Jang, X. Qiu, E. Liu, W.S. Drisdell, Z. Wei, M. Gu, K. Amine, M. Shao, *J. Am. Chem. Soc.* **2022**, *144*, 20372.

[S21] B. Liu, R. Feng, M. Busch, S. Wang, H. Wu, P. Liu, J. Gu, A. Bahadoran, D. Matsumura, T. Tsuji, D. Zhang, F. Song, Q. Liu, *ACS Nano* **2022**, *16*, 14121.

[S22] X. Zhu, X. Tan, K.H. Wu, S.C. Haw, C.W. Pao, B.J. Su, J. Jiang, S.C. Smith, J.M. Chen, R. Amal, X. Lu, *Angew. Chem. Int. Ed.* **2021**, *60*, 21911.

[S23] Z. Li, W. Niu, Z. Yang, N. Zaman, W. Samarakoon, M. Wang, A. Kara, M. Lucero, M.V. Vyas, H. Cao, H. Zhou, G.E. Sterbinsky, Z. Feng, Y. Du, Y. Yang, *Energy Environ. Sci.* **2020**, *13*, 884.